

Inadequacy of zero-width approximation for a light Higgs boson signal

Nikolas Kauer^a and Giampiero Passarino^b

^a*Department of Physics, Royal Holloway, University of London,
Egham TW20 0EX, United Kingdom*

^b*Dipartimento di Fisica Teorica, Università di Torino, Italy
INFN, Sezione di Torino, Italy*

E-mail: n.kauer@rhul.ac.uk, giampiero@to.infn.it

ABSTRACT: In the Higgs search at the LHC, a light Higgs boson ($115 \text{ GeV} \leq M_H \lesssim 130 \text{ GeV}$) is not excluded by experimental data. In this mass range, the width of the Standard Model Higgs boson is more than four orders of magnitude smaller than its mass. The zero-width approximation is hence expected to be an excellent approximation. We show that this is not always the case. The inclusion of off-shell contributions is essential to obtain an accurate Higgs signal normalisation at the 1% precision level. For $gg (\rightarrow H) \rightarrow VV$, $V = W, Z$, $\mathcal{O}(10\%)$ corrections occur due to an enhanced Higgs signal in the region $M_{VV} > 2 M_V$, where also sizable Higgs-continuum interference occurs. We discuss how experimental selection cuts can be used to exclude this region in search channels where the Higgs invariant mass cannot be reconstructed. We note that the $H \rightarrow VV$ decay modes in weak boson fusion are similarly affected.

KEYWORDS: Higgs Physics, QCD, Hadron-Hadron Scattering

Contents

1	Introduction	1
2	Inclusive analysis	2
3	Analysis with experimental selection cuts	6
3.1	$gg \rightarrow H \rightarrow ZZ \rightarrow \ell\bar{\ell}\ell\bar{\ell}$ and $\ell\bar{\ell}\ell'\bar{\ell}'$ at $M_H = 125$ GeV	7
3.2	$gg \rightarrow H \rightarrow W^-W^+ \rightarrow \ell\bar{\nu}_\ell\bar{\ell}\nu_\ell$ at $M_H = 125$ GeV	8
3.3	$gg \rightarrow H \rightarrow ZZ \rightarrow \ell\bar{\ell}\nu_\ell\bar{\nu}_\ell$ at $M_H = 200$ GeV	9
3.4	$gg \rightarrow H \rightarrow ZZ \rightarrow \ell\bar{\ell}\nu_\ell\bar{\nu}_\ell$ at $M_H = 125$ GeV	14
4	Conclusions	16

1 Introduction

In the Higgs search at the LHC, a light Higgs boson ($115 \text{ GeV} \leq M_H \lesssim 130 \text{ GeV}$) is not excluded by experimental data. The signal process (Fig. 1, left) has been calculated and studied up to NNLO (see Refs. [1–11] and references therein).

In this mass range, the on-shell width of the Standard Model (SM) Higgs boson is more than four orders of magnitude smaller than its mass, i.e. $\Gamma_H = 4.03 \text{ MeV}$ for $M_H = 125 \text{ GeV}$. The zero-width approximation (ZWA) is defined as the production cross-section for a Higgs boson on-shell followed by its (on-shell) decay. ZWA is hence expected to be an excellent approximation well below the $WW(ZZ)$ threshold. For the gluon fusion channel ($gg \rightarrow H$), we show that this is not always the case.

For $gg (\rightarrow H) \rightarrow VV$, where $V = W, Z$, the deviation of the full, off-shell, calculation from the ZWA is particularly large. We take into account the resonance-continuum interference in $gg (\rightarrow H) \rightarrow VV$, which has been studied in Refs. [12–16] and for related processes in Refs. [17, 18].

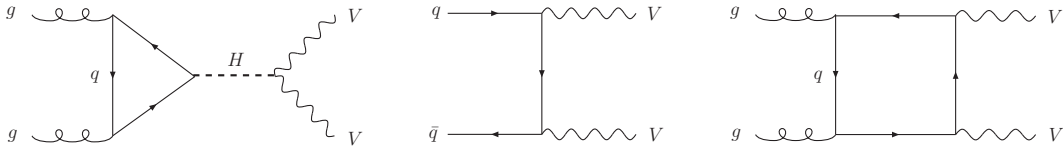


Figure 1. Representative Feynman graphs for the Higgs signal process (left) and the $q\bar{q}$ - (center) and gg -initiated (right) continuum background processes at LO.

2 Inclusive analysis

In the SM, the common belief is that for a light Higgs boson the product of on-shell production cross-section (say in gluon-gluon fusion, $gg \rightarrow H$) and branching ratios reproduces the correct result to great accuracy. The expectation is based on the well-known result

$$D_H(q^2) = \frac{1}{(q^2 - M_H^2)^2 + \Gamma_H^2 M_H^2} = \frac{\pi}{M_H \Gamma_H} \delta(q^2 - M_H^2) + PV \left[\frac{1}{(q^2 - M_H^2)^2} \right] + \sum_{n=0}^N c_n(\alpha) \delta_n(q^2 - M_H^2) \quad (2.1)$$

where q^2 is the virtuality of the Higgs boson, M_H and Γ_H are the on-shell Higgs mass and width and PV denotes the principal value (understood as a distribution). Furthermore, $\delta_n(x)$ is connected to the n th derivative of the delta-function by $\delta_n(x) = (-1)^n/n! \delta^{(n)}(x)$ and the expansion is in terms of the coupling constant, up to a given order N .

In general, ZWA can be applied to predict the probability for resonant scattering processes when the total decay width Γ of the resonant particle is much smaller than its mass M . Note that both concepts, on-shell mass and width, are ill-defined for an unstable particle and should be replaced with the complex pole, which is a property of the S -matrix, gauge-parameter independent to all orders of perturbation theory. Nevertheless, let us continue with our qualitative argument: in the limit $\Gamma \rightarrow 0$, the mod-squared propagator

$$D(q^2) = \left[(q^2 - M^2)^2 + (M\Gamma)^2 \right]^{-1} \quad (2.2)$$

with 4-momentum q approaches the delta-function limit of Eq. (2.1), i.e.

$$D(q^2) \sim K \delta(q^2 - M^2), \quad K = \frac{\pi}{M\Gamma} = \int_{-\infty}^{+\infty} dq^2 D(q^2). \quad (2.3)$$

The scattering cross-section σ thus approximately decouples into on-shell production (σ_p) and decay as shown in Eqs. (2.4)–(2.6), where s is the total 4-momentum squared, argument based on the scalar nature of the resonance. Based on the scales occurring in $D(q^2)$, the conventional error estimate is $\mathcal{O}(\Gamma/M)$. This will not be accurate when the q^2 dependence of $|\mathcal{M}_p|^2$ or $|\mathcal{M}_d|^2$ is strong enough to compete with the q^2 dependence of D . An interesting example is $gg \rightarrow H \rightarrow VV$, where $\sum |\mathcal{M}_d(q^2)|^2 \sim (q^2)^2$ above $2M_V$. For processes in SM extensions, similar effects have been studied in Refs. [19–22].

$$\sigma = \frac{1}{2s} \left[\int_{q_{\min}^2}^{q_{\max}^2} \frac{dq^2}{2\pi} \left(\int d\phi_p |\mathcal{M}_p(q^2)|^2 D(q^2) \int d\phi_d |\mathcal{M}_d(q^2)|^2 \right) \right] \quad (2.4)$$

$$\sigma_{\text{ZWA}} = \frac{1}{2s} \left(\int d\phi_p |\mathcal{M}_p(M^2)|^2 \right) \left(\int_{-\infty}^{\infty} \frac{dq^2}{2\pi} D(q^2) \right) \left(\int d\phi_d |\mathcal{M}_d(M^2)|^2 \right) \quad (2.5)$$

$$\sigma_{\text{ZWA}} = \frac{1}{2s} \left(\int d\phi_p |\mathcal{M}_p|^2 \right) \frac{1}{2M\Gamma} \left(\int d\phi_d |\mathcal{M}_d|^2 \right) \Big|_{q^2=M^2} \quad (2.6)$$

An important observation is that the Breit-Wigner distribution does not drop off nearly as fast as, for instance, a Gaussian. The relative contribution of the tail more than n widths from the peak can be estimated as $1/(n\pi)$, because [23]

$$\int_{(M-n\Gamma)^2}^{(M+n\Gamma)^2} \frac{dq^2}{2\pi} \frac{1}{(q^2 - M^2)^2 + (M\Gamma)^2} \approx \frac{1}{2M\Gamma} \left(1 - \frac{1}{n\pi}\right). \quad (2.7)$$

Since the width of a light Higgs is so small, $n = 1000$ corresponds to only a few GeV, beyond which one would expect less than 0.04% of the signal cross section.

A potential worry, addressed in this paper, is: to which level of accuracy does the ZWA approximate the full off-shell result, given that at $M_H = 125$ GeV the on-shell width (very close to the imaginary part of the complex pole) is 4.03 MeV. When searching the Higgs boson around 125 GeV one should not care about the region $M_{ZZ} > 2 M_Z$ but, due to limited statistics, theory predictions for the normalisation in $\bar{q}q - gg \rightarrow ZZ$ are used over the entire spectrum in the ZZ invariant mass.

Therefore, the question is not to dispute that off-shell effects are depressed by a factor Γ_H/M_H , as shown in Eq. (2.1), but to move away from the peak in the invariant mass distribution and look at the behavior of the distribution, no matter how small it is compared to the peak; is it really decreasing with M_{ZZ} ? Is there a plateau? For how long is the plateau lasting? How does that affect the total cross-section if no cut is made?

In this section, we consider the signal (S) in the complex-pole scheme of Refs. [24–26])

$$\sigma_{gg \rightarrow ZZ}(S) = \sigma_{gg \rightarrow H \rightarrow ZZ}(M_{ZZ}) = \frac{1}{\pi} \sigma_{gg \rightarrow H}(M_{ZZ}) \frac{M_{ZZ}^4}{|M_{ZZ}^2 - s_H|^2} \frac{\Gamma_{H \rightarrow ZZ}(M_{ZZ})}{M_{ZZ}}, \quad (2.8)$$

where s_H is the Higgs complex pole, parametrized by $s_H = \mu_H^2 - i\mu_H\gamma_H$. Note that γ_H is not the on-shell width, although the numerical difference is tiny for low values of μ_H , as shown in Ref. [24].

The production cross-section, $\sigma_{gg \rightarrow H}$, is computed with next-to-next-to-leading (NNLO) QCD corrections (see Ref. [27]) and NLO EW ones [28]. The partial decay width of the off-shell Higgs boson of virtuality M_{ZZ} ($\Gamma_{H \rightarrow ZZ}$), is at NLO with leading NNLO effects in the limit of large Higgs boson mass, see Ref. [29]. Numerical results in this Section are obtained with the program HTO (G. Passarino, unpublished) that allows for the study of the Higgs-boson-lineshape, in gluon-gluon fusion, using complex poles. Our results refer to $\sqrt{s} = 8$ TeV and are based on the MSTW2008 PDF sets [30]. They are implemented according to the OFFP - scheme, see Eq. (45) of Ref. [24]. Furthermore we use renormalisation and factorisation QCD scales that evolve with the Higgs virtuality.

Away (but not too far away) from the narrow peak the propagator and the off-shell H width behave like

$$D_H(M_{ZZ}^2) \approx \frac{1}{(M_{ZZ}^2 - \mu_H^2)^2}, \quad \frac{\Gamma_{H \rightarrow ZZ}(M_Z)}{M_{ZZ}} \sim G_F M_{ZZ}^2 \quad (2.9)$$

above threshold with a sharp increase just below it (it goes from $1.62 \cdot 10^{-2}$ GeV at 175 GeV to $1.25 \cdot 10^{-1}$ GeV at 185 GeV). Our result for the VV ($V = W, Z$) invariant mass distribution is shown in Fig. 2. It confirms that, after the peak, the distribution is falling down

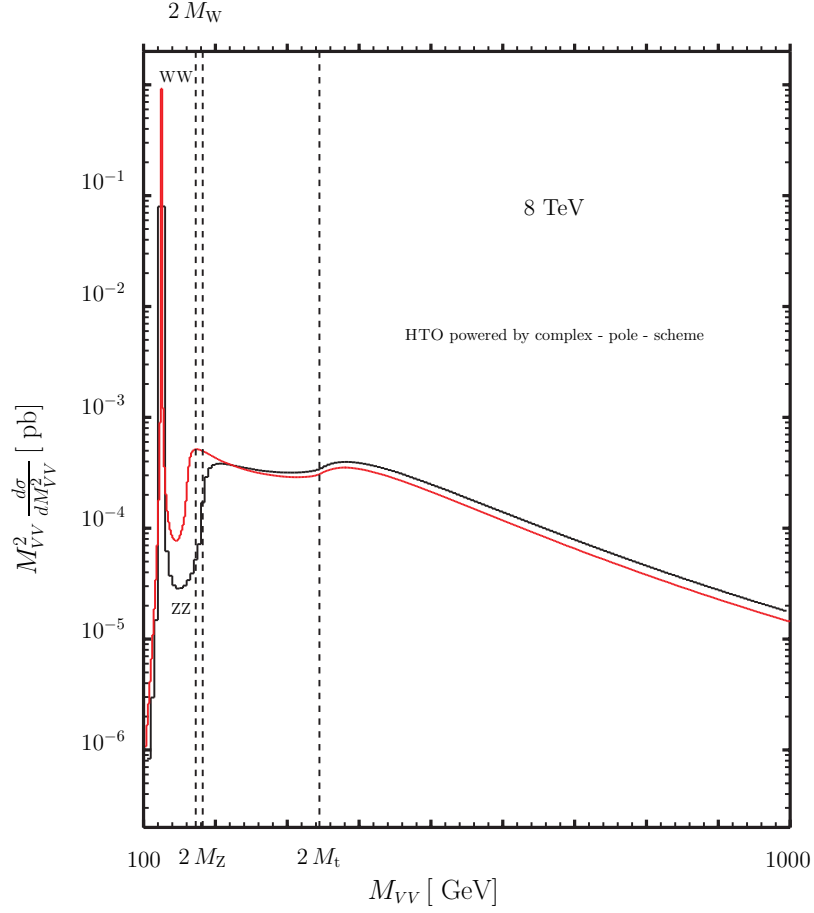


Figure 2. The NNLO ZZ (black) and WW (red) invariant mass distributions in $gg \rightarrow VV$ for $\mu_H = 125$ GeV.

until the effects of the VV -thresholds become effective with a visible increase followed by a plateau, by another jump at the $t\bar{t}$ -threshold. Finally the signal distribution starts again to decrease, almost linearly. If one looks instead for $gg \rightarrow H \rightarrow \gamma\gamma$ the effect is drastically reduced and confined to the region $M_{\gamma\gamma}$ between 157 GeV and 168 GeV where, however the distribution is already five orders of magnitude below the peak.

What is the net effect on the total cross-section? We show it for ZZ in Table 1 where the contribution above the ZZ -threshold amounts to 7.6%. We have checked that the effect does not depend on the propagator function, complex-pole propagator or Breit-Wigner distribution. However, the size of the effect is related to the shape of the distribution function. The complex-mass scheme can be translated into a more familiar language by introducing the Bar – scheme [24]. Performing the well-known transformation

$$\overline{M}_H^2 = \mu_H^2 + \gamma_H^2, \quad \mu_H \overline{\Gamma}_H = \overline{M}_H \gamma_H. \quad (2.10)$$

	Tot[pb]	$M_{ZZ} > 2 M_Z$ [pb]	R[%]
$gg \rightarrow H \rightarrow \text{all}$	19.146	0.1525	0.8
$gg \rightarrow H \rightarrow ZZ$	0.5462	0.0416	7.6

Table 1. Total cross-section for the processes $gg \rightarrow H \rightarrow ZZ$ and $gg \rightarrow H \rightarrow \text{all}$; the part of the cross-section coming from the region $M_{ZZ} > 2 M_Z$ is explicitly shown, as well as the ratio.

100–125	125–150	150–175	175–200	200–225	225–250	250–275
0.252	0.252	$0.195 \cdot 10^{-3}$	$0.177 \cdot 10^{-2}$	$0.278 \cdot 10^{-2}$	$0.258 \cdot 10^{-2}$	$0.240 \cdot 10^{-2}$

Table 2. Bin-by-bin integrated cross-section for the process $gg \rightarrow H \rightarrow ZZ$. The first row gives the bin in GeV, the second row gives the corresponding cross-section in pb.

a remarkable identity follows (defining the so-called Bar-scheme):

$$\frac{1}{M_{ZZ}^2 - s_H} = \left(1 + i \frac{\bar{\Gamma}_H}{M_H}\right) \left(M_{ZZ}^2 - \bar{M}_H^2 + i \frac{\bar{\Gamma}_H}{M_H} M_{ZZ}^2\right)^{-1}, \quad (2.11)$$

showing that the complex-pole scheme is equivalent to introducing a running width in the propagator with parameters that are not the on-shell ones. Special attention goes to the numerator in Eq. (2.11) which is essential in providing the right asymptotic behavior when $M_{ZZ} \rightarrow \infty$, as needed for cancellations with the rest of the amplitude. Therefore, it is not advisable to use a naive, running-width, Breit-Wigner distribution or to use a propagator with $M_{ZZ}^2 - M_H^2 + i M_H \Gamma_H(M_{ZZ}^2)$.

In Table 2 we present the invariant mass distribution integrated bin-by-bin.

If we take the ZWA value for the production cross-section at 8 TeV and for $\mu_H = 125$ GeV (19.146 pb) and use the branching ratio into ZZ of $2.67 \cdot 10^{-2}$ we obtain a ZWA result of 0.5203 pb with a 5% difference w.r.t. the off-shell result, fully compatible with the 7.6% effect coming from the high-energy side of the resonance.

Always from Table 1 we see that the effect is much less evident if we sum over all final states with a net effect of only 0.8%.

Of course, the signal per se is not a physical observable and one should always include background and interference. In Fig. 3 we show the complete LO result for $gg \rightarrow ZZ$ according to HTO. Numbers are shown with a cut of $0.25 M_{ZZ}$ on the momentum transverse of the Z . The large destructive effects of the interference after the resonant peak wash out the peculiar structure of the signal distribution. If one includes the region $M_{ZZ} > 2 M_Z$ in the analysis then the conclusion is: interference effects are relevant also for the low-mass region, at least for $ZZ(WW)$ final state. It is worth noting again that the whole effect on the signal has nothing to do with Γ_H/M_H effects; above the ZZ -threshold the distribution is higher than expected (although tiny w.r.t. the narrow peak) and stays constant till the $t\bar{t}$ -threshold after which we observe an almost linear decrease. This is why the total cross-section is affected (in ZZ final state) at the 5% level.

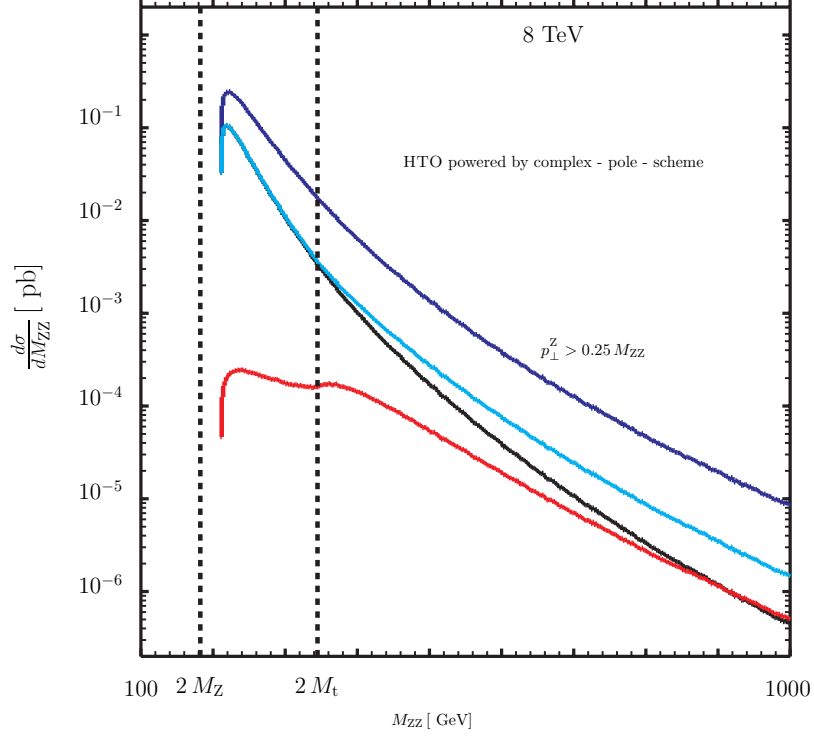


Figure 3. The LO ZZ invariant mass distribution $gg \rightarrow ZZ$ for $\mu_H = 125$ GeV. The black line is the total, the red line gives the signal while the cyan line gives signal plus background; the blue line includes the $q\bar{q} \rightarrow ZZ$ contribution.

To conclude our inclusive analysis, we note that our findings are driven by the interplay between the q^2 -dependence of the Higgs propagator and the decay matrix element. They should hence not only apply to Higgs production in gluon fusion, but also to Higgs production in weak boson fusion. The enhancement for $H \rightarrow VV$ above M_{VV} may even be stronger in weak boson fusion, because $\sigma(q\bar{q} \rightarrow q\bar{q}H)$ decreases less rapidly than $\sigma(gg \rightarrow H)$ with increasing Higgs invariant mass.

3 Analysis with experimental selection cuts

In this section, we adopt the common selection cuts definition between ATLAS and CMS for $H \rightarrow VV$ processes ($V = W, Z$) [31, 32] and calculate parton-level $gg \rightarrow H \rightarrow VV \rightarrow$ leptons cross sections at LO using gg2VV [33] based on Refs. [14, 16, 34, 35], with Higgs in ZWA as well as off-shell including interference with continuum VV production (where γ^* contributions are also included).¹ All results are given for a single lepton flavour combination. No flavour summation is carried out for charged leptons or neutrinos. As input parameters, we use the specification of the LHC Higgs Cross Section Working Group in App. A of Ref. [36] with NLO Γ_V and G_μ scheme. Finite top and bottom quark mass

¹All cross sections are evaluated with a $p_T(V) > 1$ GeV cut. This technical cut prevents numerical instabilities when evaluating the continuum amplitude.

effects are included. Lepton masses are neglected. We consider the Higgs masses 125 GeV and 200 GeV with $\Gamma_H = 0.004434$ GeV and 1.428 GeV, respectively. The Higgs widths have been calculated with HDECAY [37]. The fixed-width prescription is used for Higgs and weak boson propagators. The renormalisation and factorisation scales are set to $M_H/2$. The PDF set MSTW2008NNLO [30] with 3-loop running for $\alpha_s(\mu^2)$ and $\alpha_s(M_Z^2) = 0.11707$ is used. The CKM matrix is set to the unit matrix, which causes a negligible error [16].

The accuracy of the ZWA Higgs cross section and the impact of off-shell effects is assessed with the ratio

$$R_0 = \frac{\sigma_{H,ZWA}}{\sigma_{H,\text{offshell}}} . \quad (3.1)$$

To facilitate comparison with off-shell M_{VV} distributions, we define the ZWA M_{VV} distribution as suggested by Eq. (2.5):

$$\left(\frac{d\sigma}{dM_{VV}} \right)_{ZWA} = \sigma_{H,ZWA} \frac{M_H \Gamma_H}{\pi} \frac{2M_{VV}}{(M_{VV}^2 - M_H^2)^2 + (M_H \Gamma_H)^2} . \quad (3.2)$$

Each signal process $gg \rightarrow H \rightarrow VV \rightarrow \text{leptons}$ (with amplitude \mathcal{M}_H) and corresponding continuum background process $gg \rightarrow VV \rightarrow \text{leptons}$ (with amplitude $\mathcal{M}_{\text{cont}}$) have identical initial and final states. Hence interference occurs, and the distinction between signal and background cross sections becomes blurred:

$$|\mathcal{M}_{VV}|^2 = |\mathcal{M}_H + \mathcal{M}_{\text{cont}}|^2 = |\mathcal{M}_H|^2 + |\mathcal{M}_{\text{cont}}|^2 + 2 \text{Re}(\mathcal{M}_H \mathcal{M}_{\text{cont}}^*) . \quad (3.3)$$

We assess interference effects using a $(S + B)$ -inspired interference measure,

$$R_1 = \frac{\sigma(|\mathcal{M}_{VV}|^2)}{\sigma(|\mathcal{M}_H|^2 + |\mathcal{M}_{\text{cont}}|^2)} , \quad (3.4)$$

and a (S/\sqrt{B}) -inspired measure,

$$R_2 = \frac{\sigma(|\mathcal{M}_H|^2 + 2 \text{Re}(\mathcal{M}_H \mathcal{M}_{\text{cont}}^*))}{\sigma(|\mathcal{M}_H|^2)} . \quad (3.5)$$

In the following, charged leptons are denoted by ℓ .

3.1 $gg \rightarrow H \rightarrow ZZ \rightarrow \ell\bar{\ell}\ell\bar{\ell}$ and $\ell\bar{\ell}\ell'\bar{\ell}'$ at $M_H = 125$ GeV

The same- and different-flavour 4-charged-lepton channels have been analysed by ATLAS [38] and CMS [39] for Higgs masses in the range 110–600 GeV. In these search channels, the invariant mass of the intermediate Higgs ($M_{H^*} \equiv M_{ZZ}$) can be reconstructed. The M_{ZZ} spectrum is hence used as the discriminant variable in the final stage of the analysis, and the test statistic is evaluated with a binned maximum-likelihood fit of signal and background models to the observed M_{ZZ} distribution. For light Higgs masses, the observed M_{ZZ} distribution is dominated by experimental resolution effects and for example fitted as Gaussian with a standard deviation of 2–2.5 GeV (or similar bin sizes are used). Since the width of a light SM Higgs boson is 2–3 orders of magnitude smaller, one would expect that the ZWA is highly accurate. According to Eq. (2.7), the constraints on M_{ZZ} mentioned

$gg (\rightarrow H) \rightarrow ZZ \rightarrow 4\ell$ and $2\ell 2\ell'$							
σ [fb], pp , $\sqrt{s} = 8$ TeV, $M_H = 125$ GeV					ZWA	interference	
mode	H_{ZWA}	H_{offshell}	cont	$ H_{\text{ofs+cont}} ^2$	R_0	R_1	R_2
$\ell\bar{\ell}\ell\bar{\ell}$	0.0748(2)	0.0747(2)	0.000437(3)	0.0747(6)	1.002(3)	0.994(8)	0.994(8)
$\ell\bar{\ell}\ell'\bar{\ell}'$	0.1395(2)	0.1393(2)	0.000583(2)	0.1400(3)	1.002(2)	1.001(2)	1.001(2)

Table 3. Cross sections for $gg (\rightarrow H) \rightarrow ZZ \rightarrow \ell\bar{\ell}\ell\bar{\ell}$ and $\ell\bar{\ell}\ell'\bar{\ell}'$ in pp collisions at $\sqrt{s} = 8$ TeV for $M_H = 125$ GeV and $\Gamma_H = 0.004434$ GeV calculated at LO with gg2VV. The zero-width approximation (ZWA) and off-shell Higgs cross sections, the continuum cross section and the sum of off-shell Higgs and continuum cross sections including interference are given. The accuracy of the ZWA and the impact of off-shell effects are assessed with $R_0 = \sigma_{H,\text{ZWA}}/\sigma_{H,\text{offshell}}$. Interference effects are illustrated through $R_1 = \sigma(|\mathcal{M}_H + \mathcal{M}_{\text{cont}}|^2)/\sigma(|\mathcal{M}_H|^2 + |\mathcal{M}_{\text{cont}}|^2)$ and $R_2 = \sigma(|\mathcal{M}_H|^2 + 2\text{Re}(\mathcal{M}_H\mathcal{M}_{\text{cont}}^*))/\sigma(|\mathcal{M}_H|^2)$. γ^* contributions are included in $\mathcal{M}_{\text{cont}}$. Applied cuts: $|M_{ZZ} - M_H| < 1$ GeV, $p_{T\ell} > 5$ GeV, $|\eta_\ell| < 2.5$, $\Delta R_{\ell\ell} > 0.1$, $76 \text{ GeV} < M_{\ell\bar{\ell},12} < 106$ GeV and $15 \text{ GeV} < M_{\ell\bar{\ell},34} < 115$ GeV (see main text), $M_{\ell\bar{\ell}} > 4$ GeV. Cross sections are given for a single lepton flavour combination. No flavour summation is carried out for charged leptons or neutrinos. The integration error is given in brackets.

above introduce an error of order 0.1%. Invariant masses above $2M_Z$, where large deviations from the Breit-Wigner shape occur, are excluded by the experimental procedure. Higgs-continuum interference effects are negligible. For illustration, we compute the Higgs cross section in ZWA and off-shell including continuum interference in the vicinity of M_H , more precisely $|M_{ZZ} - M_H| < 1$ GeV. To take into account the detector acceptance, we require $p_{T\ell} > 5$ GeV and $|\eta_\ell| < 2.5$. Leptons are separated using $\Delta R_{\ell\ell} > 0.1$. Following Ref. [38], we apply the cuts $76 \text{ GeV} < M_{\ell\bar{\ell},12} < 106$ GeV and $15 \text{ GeV} < M_{\ell\bar{\ell},34} < 115$ GeV. The invariant mass of the same-flavour, opposite-sign lepton pair closest to M_Z is denoted by $M_{\ell\bar{\ell},12}$. $M_{\ell\bar{\ell},34}$ denotes the invariant mass of the remaining lepton pair. The γ^* singularity for vanishing virtuality is excluded by requiring $M_{\ell\bar{\ell}} > 4$ GeV.² The results are displayed in Table 3.

3.2 $gg \rightarrow H \rightarrow W^-W^+ \rightarrow \ell\bar{\nu}_\ell\bar{\ell}\nu_\ell$ at $M_H = 125$ GeV

The $WW \rightarrow 2\ell 2\nu$ search channel has been analysed by ATLAS [40] and CMS [41] for Higgs masses in the range 110–600 GeV. We apply the standard cuts $p_{T\ell} > 20$ GeV, $|\eta_\ell| < 2.5$, $p_T > 30$ GeV and $M_{\ell\ell} > 12$ GeV. As Higgs search selection cuts, we apply the standard cuts and in addition $M_{\ell\ell} < 50$ GeV and $\Delta\phi_{\ell\ell} < 1.8$. Since M_{H^*} cannot be reconstructed, ATLAS and CMS also use transverse mass observables M_T that aim at approximating M_{H^*} . Ref. [40] uses the transverse mass definition³

$$M_{T1} = \sqrt{(M_{T,\ell\ell} + \not{p}_T)^2 - (\mathbf{p}_{T,\ell\ell} + \mathbf{\not{p}}_T)^2} \quad (3.6)$$

²This cut is induced by the phase space generation.

³ In the absence of additional observed final state particles, the expressions for M_T simplify due to $\mathbf{\not{p}}_T = -\mathbf{p}_{T,\ell\ell}$.

with

$$M_{T,\ell\ell} = \sqrt{p_{T,\ell\ell}^2 + M_{\ell\ell}^2} \quad (3.7)$$

and applies a $0.75M_H < M_{T1} < M_H$ cut for $M_H = 125$ GeV. Ref. [41] uses the transverse mass definition

$$M_{T2} = \sqrt{2 p_{T,\ell\ell} \not{p}_T (1 - \cos \Delta\phi_{\ell\ell,\text{miss}})}, \quad (3.8)$$

where $\Delta\phi_{\ell\ell,\text{miss}}$ is the angle between $\mathbf{p}_{T,\ell\ell}$ and $\not{\mathbf{p}}_T$, and applies a $80 \text{ GeV} < M_{T2} < M_H$ cut for $M_H = 125$ GeV.

Cross sections are presented in Table 4. When standard cuts are applied, the phase space region where $M_{WW} > 160$ GeV, or equivalently $M_{WW} > M_H + 7000\Gamma_H$, contributes 16% to the off-shell Higgs cross section. The error of the ZWA exceeds 15%, and interference effects are of $\mathcal{O}(10\%)$. Figs. 4 and 5 illustrate that the region with $M_{WW} > 2M_W$ is responsible for the inaccuracy of the ZWA as well as the unexpectedly large interference effects, in agreement with our discussion in Sec. 2. Fig. 6 demonstrates that finite-width effects and Higgs-continuum interference are negligible in the resonance region, i.e. $|M_{WW} - M_H| \lesssim \Gamma_H$, for a Higgs mass of 125 GeV. The Higgs search selection has additional cuts, in particular an upper bound on the invariant mass of the observed dilepton system, which significantly reduce the contribution from the region with $M_{WW} \gg 2M_W$, as seen in Fig. 7. The result is a substantial mitigation of the finite-width and interference effects as seen in Table 4.

We now consider the impact of cuts on transverse mass observables, which are designed to have the physical mass of the decaying parent particle (the invariant mass in the off-shell case) as upper bound [42].⁴ For the process considered here, this is shown in Fig. 8. Evidently, imposing a cut $M_T < M_H$ is an effective means to suppress interference effects. This was first noticed and studied for the M_{T1} variable in Ref. [15]. In Table 4, one can see that both, M_{T1} and M_{T2} , are suitable transverse mass variables, with M_{T1} being slightly more effective. This is also borne out by the transverse mass distributions in Figs. 9 and 10. With regard to the ZWA, Table 4 shows that the application of the M_{T1} or M_{T2} cut reduces the ZWA error to the sub-percent level.

3.3 $gg \rightarrow H \rightarrow ZZ \rightarrow \ell\bar{\ell}\nu_\ell\bar{\nu}_\ell$ at $M_H = 200$ GeV

The $ZZ \rightarrow 2\ell 2\nu$ search channel has been analysed by ATLAS [43] and CMS [44] for Higgs masses in the range 200–600 GeV. In this section we focus on the lowest studied Higgs mass of 200 GeV with $\Gamma_H/M_H = 0.7\%$. Note that M_H is slightly above the Z pair production threshold. A clean separation of the Higgs resonance and the region with large continuum background is thus not possible. We apply the Higgs search cuts $p_{T\ell} > 20$ GeV, $|\eta_\ell| < 2.5$, $76 \text{ GeV} < M_{\ell\ell} < 106 \text{ GeV}$, $\not{p}_T > 10 \text{ GeV}$ and $\Delta\phi_{\ell\ell} > 1$. Refs. [43] and [44] use a transverse mass distribution as final discriminant in searching for an excess of data over the SM background expectation. Ref. [44] employs the transverse mass variable first proposed

⁴We note that M_{T1} is referred to as M_T^{true} in Ref. [42].

	$gg (\rightarrow H) \rightarrow W^-W^+ \rightarrow \ell\bar{\nu}_\ell\bar{\ell}\nu_\ell$				ZWA	interference	
	σ [fb], pp , $\sqrt{s} = 8$ TeV, $M_H = 125$ GeV						
selection cuts	H_{ZWA}	H_{offshell}	cont	$ H_{\text{ofs}}+\text{cont} ^2$	R_0	R_1	R_2
standard cuts	2.707(3)	3.225(3)	10.493(5)	12.241(8)	0.839(2)	0.8923(7)	0.542(3)
Higgs search cuts	1.950(1)	1.980(1)	2.705(2)	4.497(3)	0.9850(7)	0.9599(7)	0.905(2)
$0.75M_H < M_{T1} < M_H$	1.7726(9)	1.779(1)	0.6443(9)	2.383(2)	0.9966(8)	0.983(1)	0.977(2)
$80 \text{ GeV} < M_{T2} < M_H$	1.7843(9)	1.794(1)	0.955(1)	2.687(3)	0.9944(8)	0.977(1)	0.965(2)

Table 4. Cross sections for $gg (\rightarrow H) \rightarrow W^-W^+ \rightarrow \ell\bar{\nu}_\ell\bar{\ell}\nu_\ell$ for $M_H = 125$ GeV with standard cuts, Higgs search cuts and additional transverse mass cut (either on M_{T1} or M_{T2}). Standard cuts: $p_{T\ell} > 20$ GeV, $|\eta_\ell| < 2.5$, $p_T > 30$ GeV, $M_{\ell\ell} > 12$ GeV. Higgs search cuts: standard cuts and $M_{\ell\ell} < 50$ GeV, $\Delta\phi_{\ell\ell} < 1.8$. M_{T1} and M_{T2} are defined in Eqs. (3.6) and (3.8) in the main text. Other details as in Table 3.

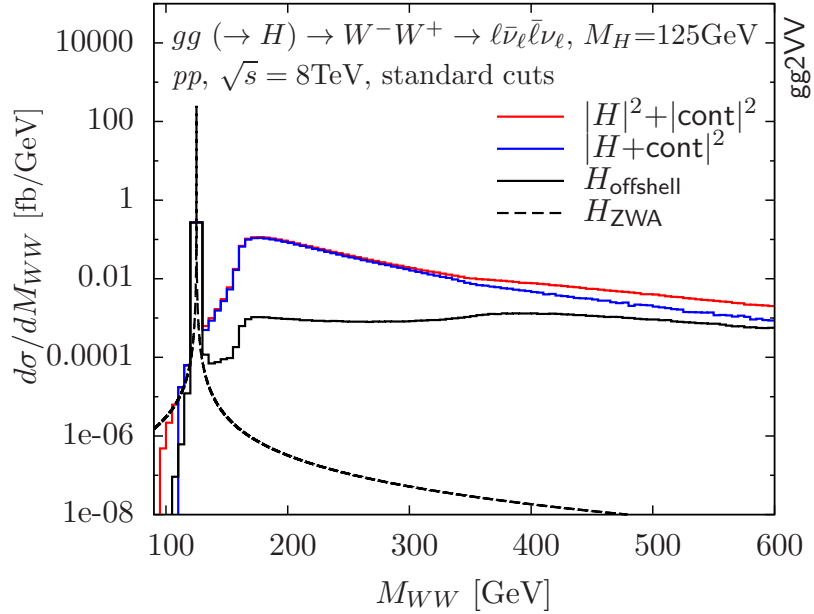


Figure 4. M_{WW} distributions for $gg (\rightarrow H) \rightarrow W^-W^+ \rightarrow \ell\bar{\nu}_\ell\bar{\ell}\nu_\ell$ in pp collisions at $\sqrt{s} = 8$ TeV for $M_H = 125$ GeV and $\Gamma_H = 0.004434$ GeV calculated at LO with gg2VV. The ZWA distribution (black, dashed) as defined in Eq. (3.2) in the main text, the off-shell Higgs distribution (black, solid), the $d\sigma(|\mathcal{M}_H + \mathcal{M}_{\text{cont}}|^2)/dM_{WW}$ distribution (blue) and the $d\sigma(|\mathcal{M}_H|^2 + |\mathcal{M}_{\text{cont}}|^2)/dM_{WW}$ distribution (red) are shown. Standard cuts are applied: $p_{T\ell} > 20$ GeV, $|\eta_\ell| < 2.5$, $p_T > 30$ GeV, $M_{\ell\ell} > 12$ GeV. Differential cross sections for a single lepton flavour combination are displayed. No flavour summation is carried out for charged leptons or neutrinos.

in Ref. [45] for the weak boson fusion $H \rightarrow WW$ channel:

$$M_{T3} = \sqrt{(M_{T,\ell\ell} + M_T)^2 - (\mathbf{p}_{T,\ell\ell} + \mathbf{p}_T)^2} \quad (3.9)$$

with $M_{T,\ell\ell}$ defined in Eq. (3.7) and

$$M_T = \sqrt{\mathbf{p}_T^2 + M_{\ell\ell}^2} \quad (3.10)$$

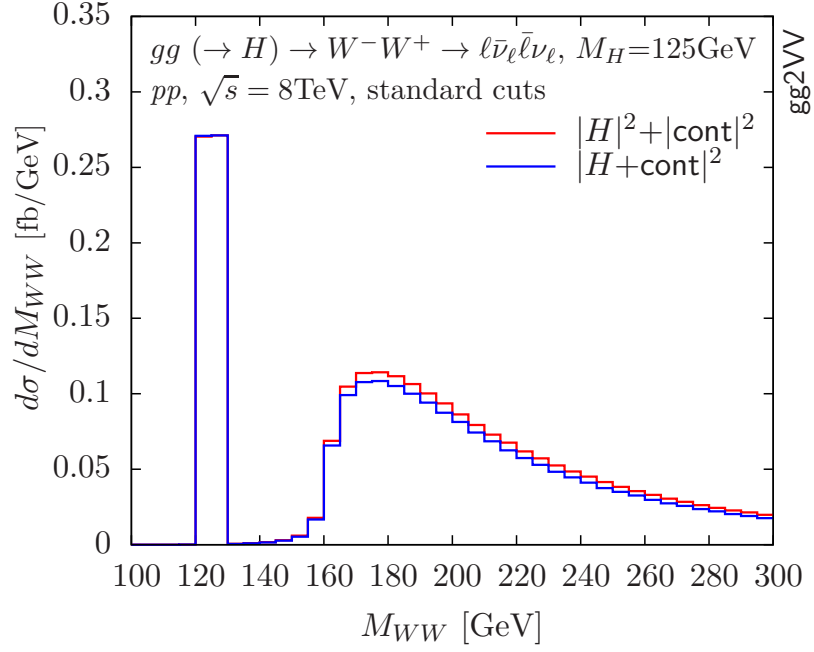


Figure 5. M_{WW} distributions for $gg(\rightarrow H) \rightarrow W^-W^+ \rightarrow \ell\bar{\nu}_\ell\ell\nu_\ell$ for $M_H = 125$ GeV. Interference effects in the region of the Higgs resonance and the W -pair threshold are shown. Details as in Fig. 4.

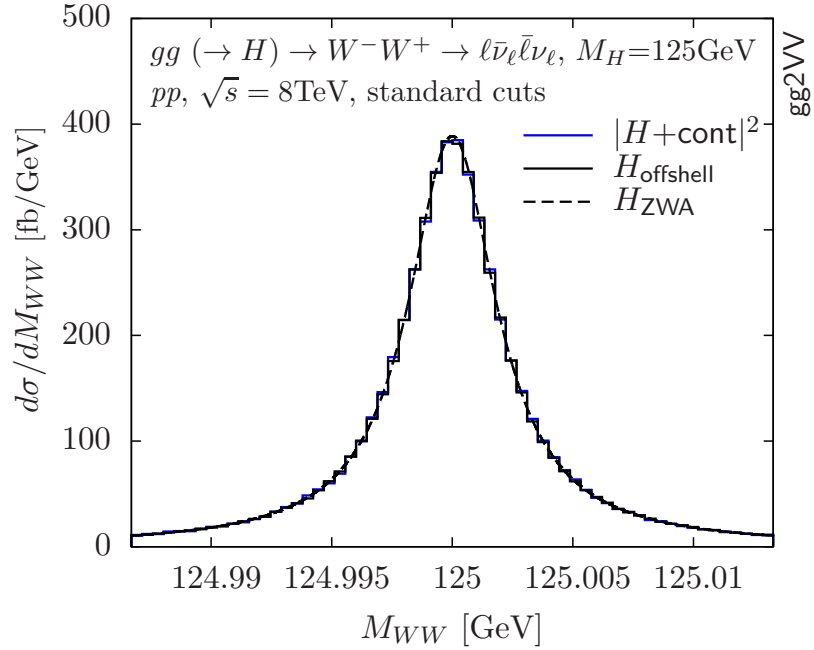


Figure 6. M_{WW} distributions for $gg(\rightarrow H) \rightarrow W^-W^+ \rightarrow \ell\bar{\nu}_\ell\ell\nu_\ell$ for $M_H = 125$ GeV. Off-shell and interference effects in the vicinity of the Higgs resonance are shown. Details as in Fig. 4.

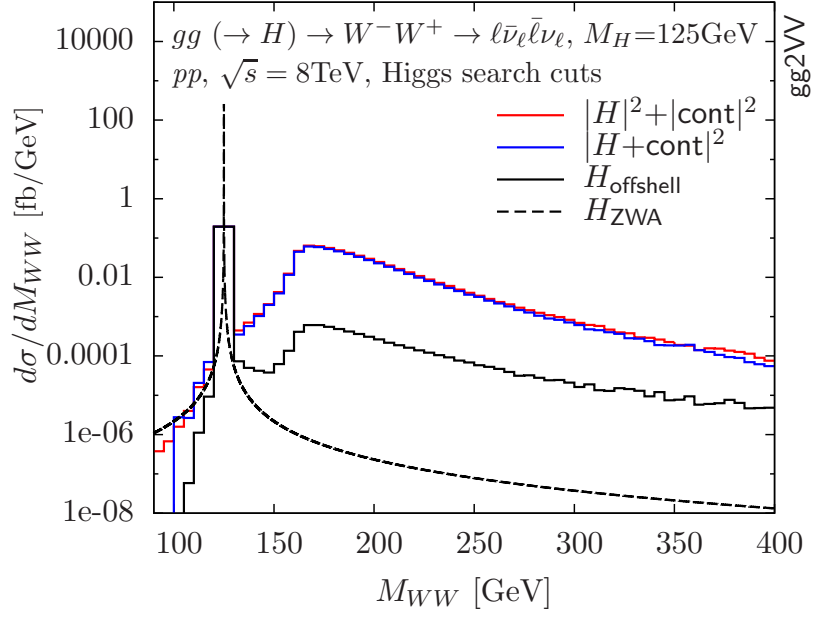


Figure 7. M_{WW} distributions for $gg (\rightarrow H) \rightarrow W^-W^+ \rightarrow \ell\bar{\nu}_\ell\bar{\ell}\nu_\ell$ for $M_H = 125$ GeV. Higgs search cuts are applied: $p_{T\ell} > 20$ GeV, $|\eta_\ell| < 2.5$, $p_T > 30$ GeV, $12 \text{ GeV} < M_{\ell\ell} < 50$ GeV, $\Delta\phi_{\ell\ell} < 1.8$. Other details as in Fig. 4.

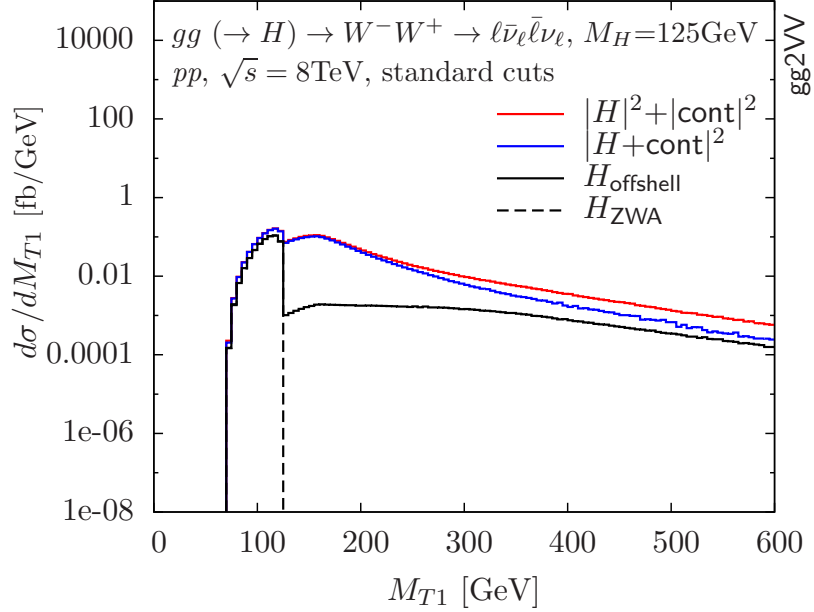


Figure 8. Transverse mass distributions for $gg (\rightarrow H) \rightarrow W^-W^+ \rightarrow \ell\bar{\nu}_\ell\bar{\ell}\nu_\ell$ for $M_H = 125$ GeV. M_{T1} is defined in Eq. (3.6) in the main text. Other details as in Fig. 4.

Note that M_{T3} , unlike M_{T1} and M_{T2} , does not have a kinematic edge at M_{H^*} . The variable used in Ref. [43] is obtained by replacing $M_{\ell\ell}$ with M_Z in the definition of M_{T3} , which

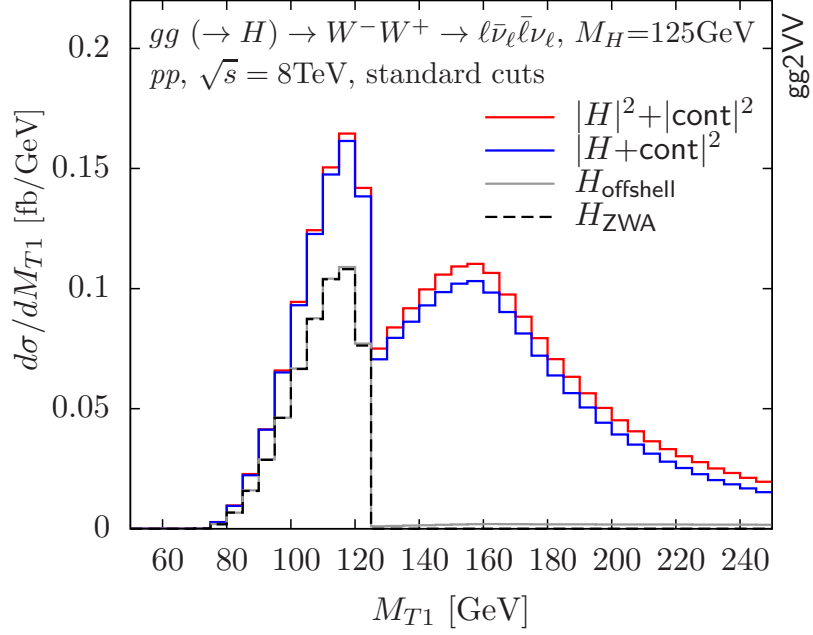


Figure 9. M_{T1} distributions for $gg (\rightarrow H) \rightarrow W^-W^+ \rightarrow \ell\bar{\nu}_\ell\ell\nu_\ell$ for $M_H = 125$ GeV. Off-shell and interference effects in the region of the Higgs resonance and the W -pair threshold are shown. M_{T1} is defined in Eq. (3.6) in the main text. Other details as in Fig. 4.

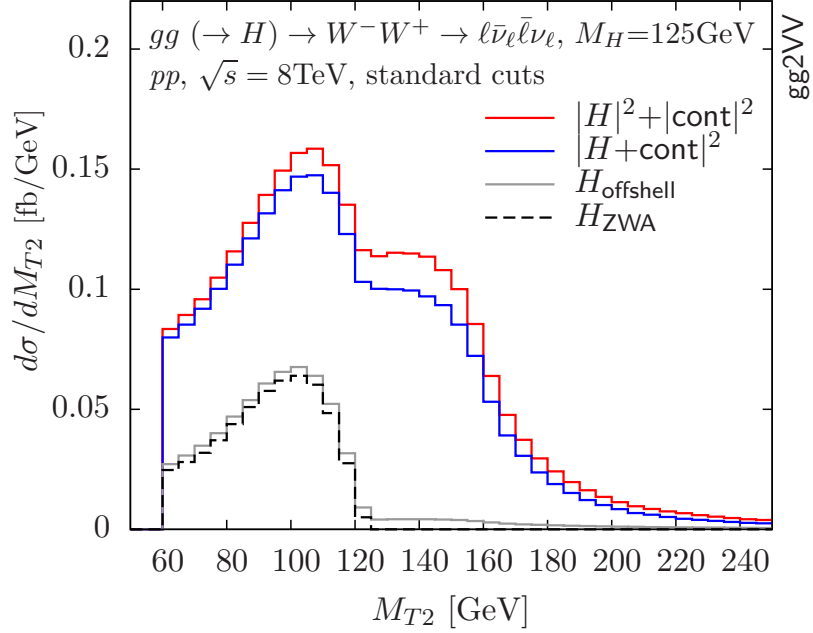


Figure 10. M_{T2} distributions for $gg (\rightarrow H) \rightarrow W^-W^+ \rightarrow \ell\bar{\nu}_\ell\ell\nu_\ell$ for $M_H = 125$ GeV. Off-shell and interference effects in the region of the Higgs resonance and the W -pair threshold are shown. M_{T2} is defined in Eq. (3.8) in the main text. Other details as in Fig. 4.

$gg (\rightarrow H) \rightarrow ZZ \rightarrow \ell\bar{\ell}\nu_\ell\bar{\nu}_\ell$						
σ [fb], pp , $\sqrt{s} = 8$ TeV, $M_H = 200$ GeV				ZWA	interference	
H_{ZWA}	H_{offshell}	cont	$ H_{\text{ofs}} + \text{cont} ^2$	R_0	R_1	R_2
2.0357(8)	2.0608(9)	1.1888(6)	3.380(2)	0.9878(6)	1.0400(7)	1.063(1)

Table 5. Cross sections for $gg (\rightarrow H) \rightarrow ZZ \rightarrow \ell\bar{\ell}\nu_\ell\bar{\nu}_\ell$ for $M_H = 200$ GeV and $\Gamma_H = 1.428$ GeV. Applied cuts: $p_{T\ell} > 20$ GeV, $|\eta_\ell| < 2.5$, $76 \text{ GeV} < M_{\ell\ell} < 106$ GeV, $p_T > 10$ GeV, $\Delta\phi_{\ell\ell} > 1$. Other details as in Table 3.

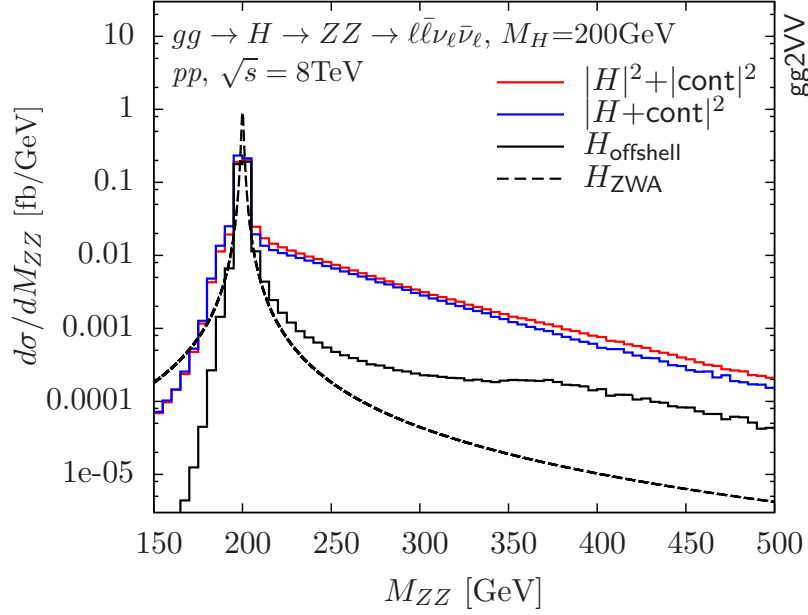


Figure 11. M_{ZZ} distributions for $gg \rightarrow H \rightarrow ZZ \rightarrow \ell\bar{\ell}\nu_\ell\bar{\nu}_\ell$ for $M_H = 200$ GeV and $\Gamma_H = 1.428$ GeV. Applied cuts: $p_{T\ell} > 20$ GeV, $|\eta_\ell| < 2.5$, $76 \text{ GeV} < M_{\ell\ell} < 106$ GeV, $p_T > 10$ GeV, $\Delta\phi_{\ell\ell} > 1$. Other details as in Fig. 4.

causes only minor differences for $M_H > 2M_Z$. No M_T cut is applied in the analyses.

In Table 5, cross section results are given. The ZWA is accurate at the percent level. Fig. 11 reveals that the off-shell enhancement of the high M_{H^*} tail is moderate. Higgs-continuum interference is constructive and of $\mathcal{O}(5\%)$. Significant interference occurs in the vicinity of the Higgs resonance as shown in Figs. 12 and 13. ZZ interference effects are comparable to WW interference effects for similar Higgs masses [14, 15]. The M_{T3} distributions displayed in Fig. 14 show that sizable ZWA deviations occur at the differential level.

3.4 $gg \rightarrow H \rightarrow ZZ \rightarrow \ell\bar{\ell}\nu_\ell\bar{\nu}_\ell$ at $M_H = 125$ GeV

Given the rapid increase in integrated luminosity at the LHC, the $ZZ \rightarrow 2\ell 2\nu$ mode could also be of interest at $M_H = 125$ GeV. We therefore extend our study to this Higgs mass. The following selection cuts are applied: $p_{T\ell} > 20$ GeV, $|\eta_\ell| < 2.5$, $76 \text{ GeV} < M_{\ell\ell} < 106$ GeV

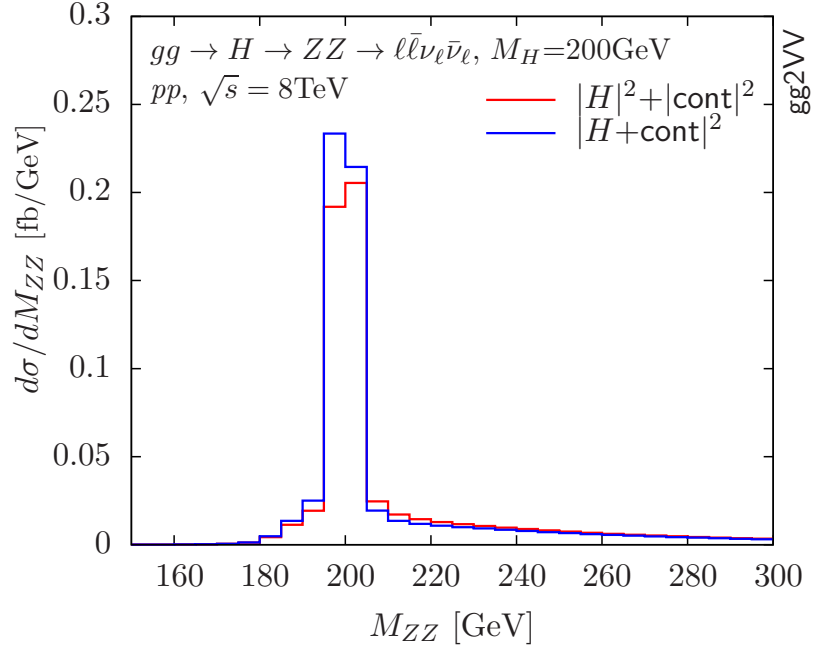


Figure 12. M_{ZZ} distributions for $gg \rightarrow H \rightarrow ZZ \rightarrow \ell\bar{\ell}\nu_\ell\bar{\nu}_\ell$ for $M_H = 200$ GeV. Interference effects in the region of the Higgs resonance and the Z -pair threshold are shown. Details as in Fig. 11.

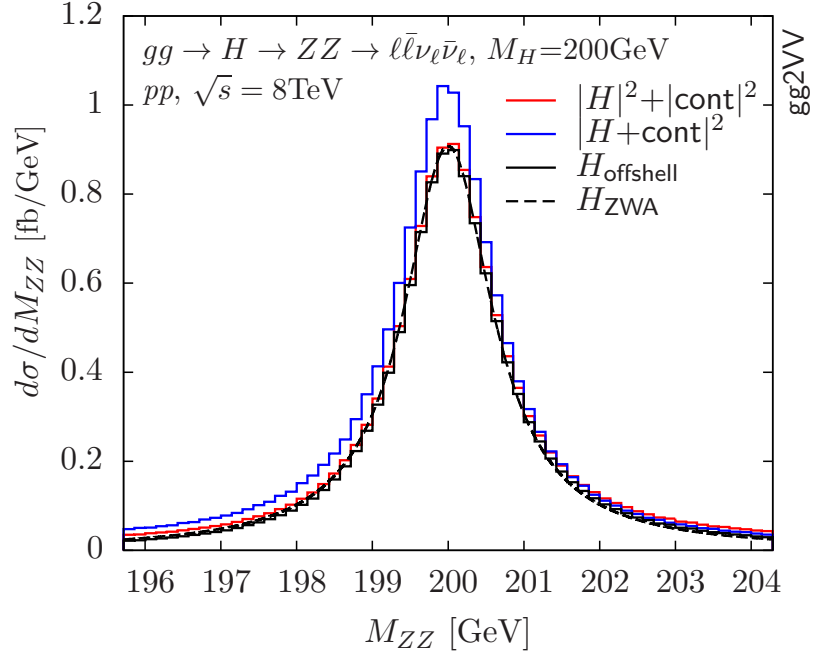


Figure 13. M_{ZZ} distributions for $gg \rightarrow H \rightarrow ZZ \rightarrow \ell\bar{\ell}\nu_\ell\bar{\nu}_\ell$ for $M_H = 200$ GeV. Off-shell and interference effects in the vicinity of the Higgs resonance are shown. Details as in Fig. 11.

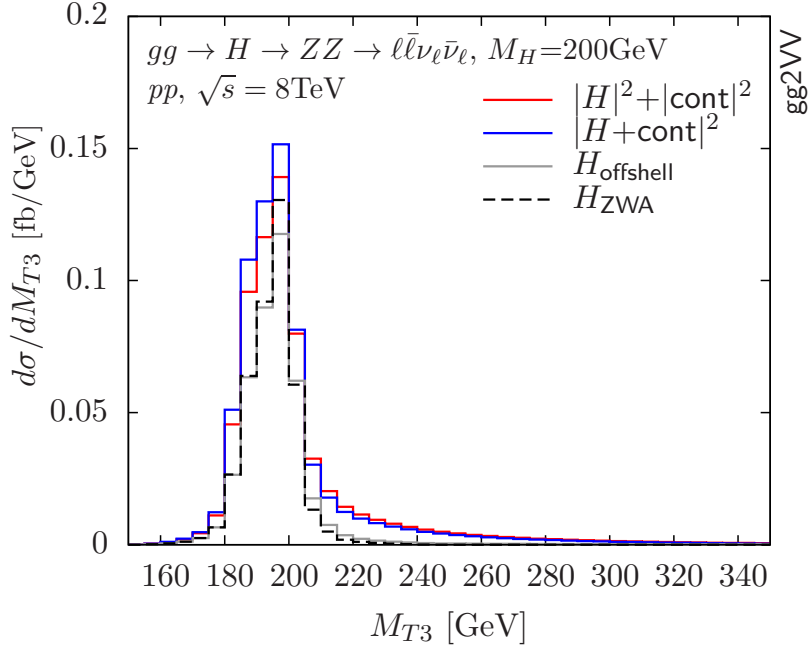


Figure 14. Transverse mass distributions for $gg \rightarrow H \rightarrow ZZ \rightarrow \ell\bar{\ell}\nu_\ell\bar{\nu}_\ell$ for $M_H = 200$ GeV. M_{T3} is defined in Eq. (3.9) in the main text. Other details as in Fig. 11.

and $\cancel{p}_T > 10$ GeV. As seen in Fig. 15, the off-shell enhancement of the high M_{H^*} tail is particularly pronounced. In Table 6, cross section results are given. The phase space region where $M_{ZZ} > 180$ GeV, or equivalently $M_{ZZ} > M_H + 12000\Gamma_H$, contributes 37% to the off-shell Higgs cross section. The ZWA underestimates the Higgs cross section by a similar amount. Figs. 15 and 16 illustrate that the region with $M_{ZZ} > 2M_Z$ is also responsible for interference effects of $\mathcal{O}(10\%)$. Fig. 17 demonstrates that finite-width effects and Higgs-continuum interference are negligible in the resonance region.

To mitigate the impact of the M_{H^*} region with large ZWA deviations and Higgs-continuum interference, we propose to employ a $M_{T1} < M_H$ cut. With this cut, the off-shell and interference effects (R_1) are reduced to the 2% level. The M_{T1} distribution displayed in Fig. 18 shows that the contamination of the $M_{T1} < M_H$ region from the interference-inducing $M_{H^*} > 2M_Z$ region is more severe than in the WW case (compare Fig. 9).

4 Conclusions

In the Higgs search at the LHC, a light Higgs boson ($115 \text{ GeV} \leq M_H \lesssim 130 \text{ GeV}$) is not excluded by experimental data. In this mass range, the width of the SM Higgs boson is more than four orders of magnitude smaller than its mass. The zero-width approximation is hence expected to be an excellent approximation. We show that this is not always the case. The inclusion of off-shell contributions is essential to obtain an accurate Higgs signal normalisation at the 1% precision level. For $gg (\rightarrow H) \rightarrow VV$, $\mathcal{O}(10\%)$ corrections

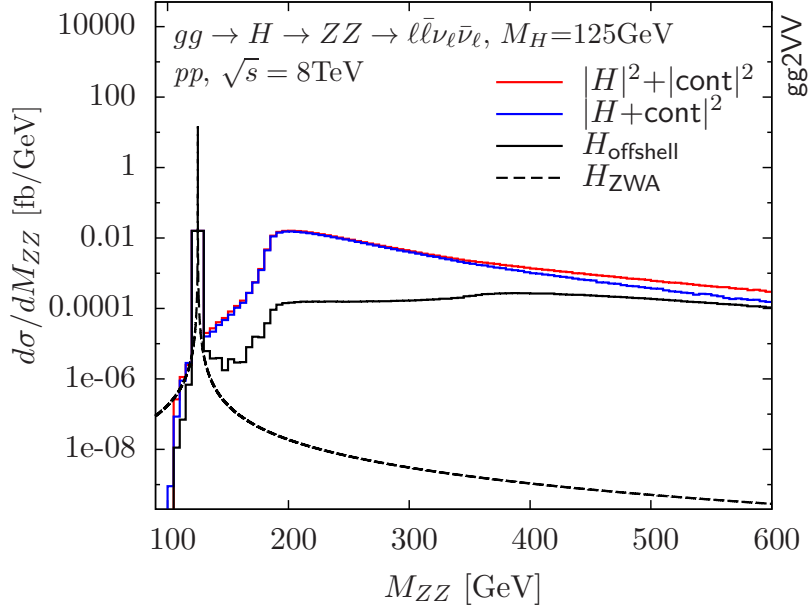


Figure 15. M_{ZZ} distributions for $gg \rightarrow H \rightarrow ZZ \rightarrow \ell\bar{\ell}\nu_\ell\bar{\nu}_\ell$ for $M_H = 125$ GeV. Applied cuts: $p_{T\ell} > 20$ GeV, $|\eta_\ell| < 2.5$, $76 \text{ GeV} < M_{\ell\ell} < 106 \text{ GeV}$, $p_T > 10$ GeV. Other details as in Fig. 4.

	$gg\,(\rightarrow H)\rightarrow ZZ\rightarrow \ell\bar{\ell}\nu_\ell\bar{\nu}_\ell$						
	$\sigma\,[\text{fb}],\,pp,\,\sqrt{s}=8\,\text{TeV},\,M_H=125\,\text{GeV}$				ZWA	interference	
M_T cut	H_{ZWA}	H_{offshell}	cont	$ H_{\text{ofs}}+\text{cont} ^2$	R_0	R_1	R_2
none	0.1593(2)	0.2571(2)	1.5631(7)	1.6376(9)	0.6196(7)	0.8997(6)	0.290(5)
$M_{T1} < M_H$	0.1593(2)	0.1625(2)	0.4197(5)	0.5663(6)	0.980(2)	0.973(2)	0.902(5)

Table 6. Cross sections for $gg (\rightarrow H) \rightarrow ZZ \rightarrow \ell\bar{\ell}\nu_\ell\bar{\nu}_\ell$ for $M_H = 125$ GeV without and with transverse mass cut. Applied cuts: $p_{T\ell} > 20$ GeV, $|\eta_\ell| < 2.5$, $76 \text{ GeV} < M_{\ell\ell} < 106 \text{ GeV}$, $p_T > 10$ GeV. Other details as in Table 3.

occur due to an enhanced Higgs signal in the region $M_{VV} > 2M_V$, where also sizable Higgs-continuum interference occurs. We discuss how experimental selection cuts can be used to exclude this region in search channels where the Higgs invariant mass cannot be reconstructed. We note that the $H \rightarrow VV$ decay modes in weak boson fusion are similarly affected. Finally, if a SM light Higgs signal will be confirmed, the next step in the analysis will be the extraction of the Higgs couplings and properties. This study will be performed using the ZWA with a consequent error of $\mathcal{O}(5\%)$ on the couplings. Although this is still tolerable with current statistics, it is obvious that the on-shell effect has to be included in future analyses.

In summary, we have shown that every off-shell calculation will reproduce the long-tail effect in the invariant-mass distribution and one should be aware of it and, eventually, decide to apply cuts. The latter is motivated by the fact that, intuitively, we would not like to assign events with large invariant mass to a low mass Higgs signal, but they are

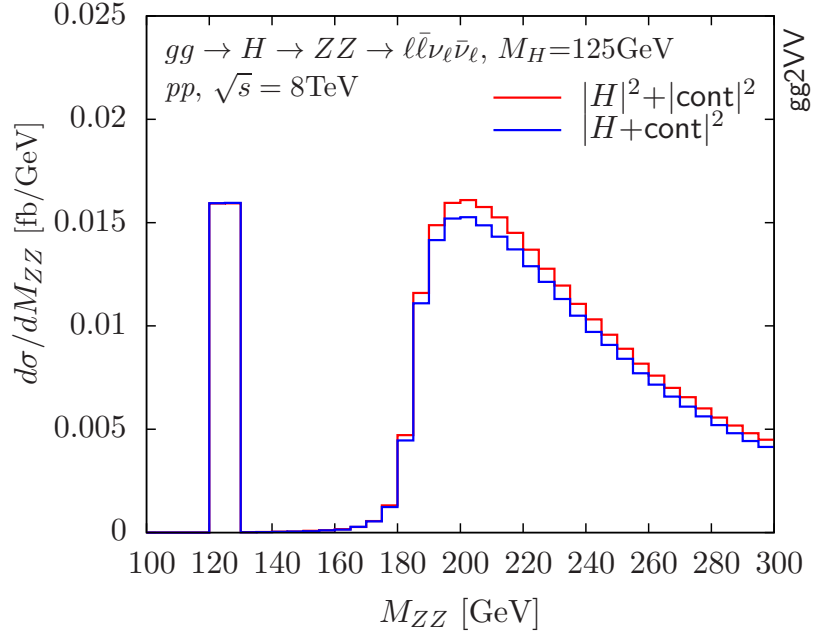


Figure 16. M_{ZZ} distributions for $gg \rightarrow H \rightarrow ZZ \rightarrow \ell\bar{\ell}\nu_\ell\bar{\nu}_\ell$ for $M_H = 125$ GeV. Interference effects in the region of the Higgs resonance and the Z -pair threshold are shown. Details as in Fig. 15.

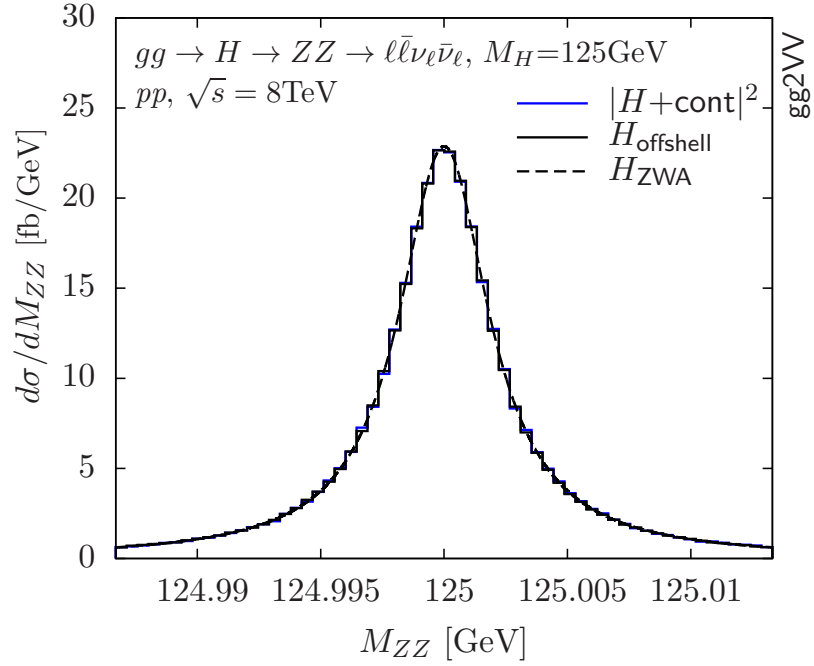


Figure 17. M_{ZZ} distributions for $gg \rightarrow H \rightarrow ZZ \rightarrow \ell\bar{\ell}\nu_\ell\bar{\nu}_\ell$ for $M_H = 125$ GeV. Off-shell and interference effects in the vicinity of the Higgs resonance are shown. Details as in Fig. 15.

there. We can also say that, “a posteriori”, the use of a ZWA is equivalent to a cut on

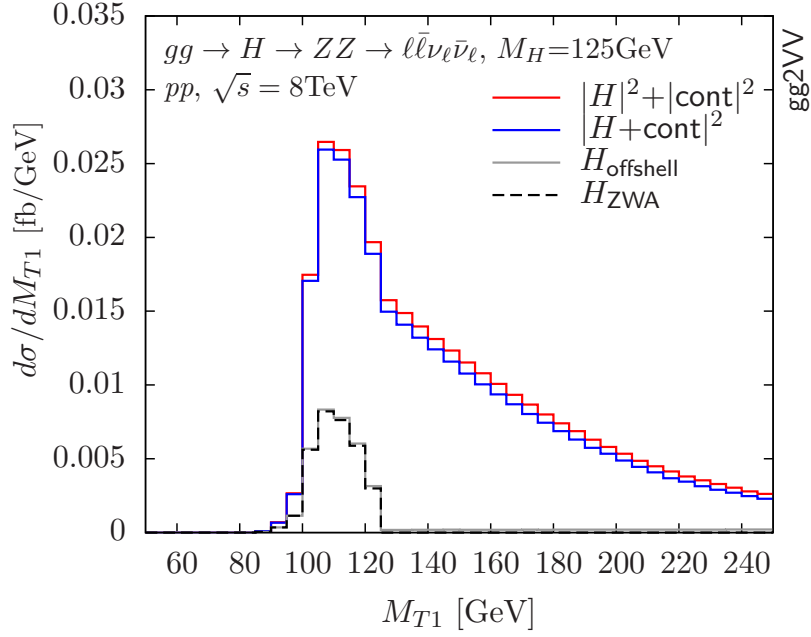


Figure 18. Transverse mass distributions for $gg \rightarrow H \rightarrow ZZ \rightarrow \ell\bar{\ell}\nu_\ell\bar{\nu}_\ell$ for $M_H = 125$ GeV. M_{T1} is defined in Eq. (3.6) in the main text. Other details as in Fig. 15.

the invariant mass, but the cut remains unspecified. In any case, there should be no claim of $\mathcal{O}(1\%)$ precision in using the ZWA. It is worth noting that we made no statement on detectability of a large invariant mass signal due to a low-mass Higgs boson, due to a huge background and interference effects. The problem remains to identify where experiments actually use, implicitly or explicitly, ZWA and correct for it.

Acknowledgments

We would like to thank the conveners and members of the LHC Higgs Cross Section Working Group for stimulating and informative discussions. N.K. would like to thank M. Rodgers for useful comparisons. G.P.’s work is supported by MIUR under contract 2001023713_006 and by Compagnia di San Paolo under contract ORTO11TPXK. Financial support from the Higher Education Funding Council for England, the Science and Technology Facilities Council and the Institute for Particle Physics Phenomenology, Durham, is gratefully acknowledged by N.K.

References

- [1] A. Djouadi, M. Spira and P. M. Zerwas, *Production of Higgs bosons in proton colliders: QCD corrections*, Phys. Lett. B **264** (1991) 440.
- [2] S. Dawson, *Radiative corrections to Higgs boson production*, Nucl. Phys. B **359** (1991) 283.
- [3] M. Spira, A. Djouadi, D. Graudenz and P. M. Zerwas, *Higgs boson production at the LHC*, Nucl. Phys. B **453** (1995) 17 [hep-ph/9504378].

- [4] R. V. Harlander and W. B. Kilgore, *Next-to-next-to-leading order Higgs production at hadron colliders*, Phys. Rev. Lett. **88** (2002) 201801 [hep-ph/0201206].
- [5] C. Anastasiou and K. Melnikov, *Higgs boson production at hadron colliders in NNLO QCD*, Nucl. Phys. B **646** (2002) 220 [arXiv:hep-ph/0207004].
- [6] V. Ravindran, J. Smith and W. L. van Neerven, *NNLO corrections to the total cross section for Higgs boson production in hadron-hadron collisions*, Nucl. Phys. B **665** (2003) 325 [arXiv:hep-ph/0302135].
- [7] C. Anastasiou, K. Melnikov and F. Petriello, *Higgs boson production at hadron colliders: differential cross sections through next-to-next-to-leading order*, Phys. Rev. Lett. **93** (2004) 262002 [arXiv:hep-ph/0409088].
- [8] C. Anastasiou, G. Dissertori and F. Stockli, *NNLO QCD predictions for the $H \rightarrow WW \rightarrow \ell\nu\ell\nu$ signal at the LHC*, JHEP **0709** (2007) 018 [arXiv:0707.2373 [hep-ph]].
- [9] S. Catani and M. Grazzini, *A NNLO subtraction formalism in hadron collisions and its application to Higgs boson production at the LHC*, Phys. Rev. Lett. **98** (2007) 222002 [arXiv:hep-ph/0703012].
- [10] M. Grazzini, *NNLO predictions for the Higgs boson signal in the $H \rightarrow WW \rightarrow \ell\nu\ell\nu$ and $H \rightarrow ZZ \rightarrow 4\ell$ decay channels*, JHEP **0802** (2008) 043 [arXiv:0801.3232 [hep-ph]].
- [11] C. Anastasiou, S. Buehler, F. Herzog and A. Lazopoulos, *Total cross section for Higgs boson hadroproduction with anomalous Standard Model interactions*, JHEP **1112** (2011) 058 [arXiv:1107.0683 [hep-ph]].
- [12] E. W. N. Glover and J. J. van der Bij, *Vector boson pair production via gluon fusion*, Phys. Lett. B **219** (1989) 488.
- [13] E. W. N. Glover and J. J. van der Bij, *Z-boson pair production via gluon fusion*, Nucl. Phys. B **321** (1989) 561.
- [14] T. Binoth, M. Ciccolini, N. Kauer and M. Kramer, *Gluon-induced W-boson pair production at the LHC*, JHEP **0612** (2006) 046 [hep-ph/0611170].
- [15] J. M. Campbell, R. K. Ellis and C. Williams, *Gluon-gluon contributions to W^+W^- production and Higgs interference effects*, JHEP **1110** (2011) 005 [arXiv:1107.5569 [hep-ph]].
- [16] N. Kauer, *Signal-background interference in $gg \rightarrow H \rightarrow VV$* , arXiv:1201.1667 [hep-ph].
- [17] L. J. Dixon and M. S. Siu, *Resonance-continuum interference in the diphoton Higgs signal at the LHC*, Phys. Rev. Lett. **90** (2003) 252001 [hep-ph/0302233].
- [18] L. J. Dixon and Y. Sofianatos, *Resonance-continuum interference in light Higgs boson production at a photon collider*, Phys. Rev. D **79** (2009) 033002 [arXiv:0812.3712 [hep-ph]].
- [19] D. Berdine, N. Kauer and D. Rainwater, *Breakdown of the narrow-width approximation for New Physics*, Phys. Rev. Lett. **99** (2007) 111601 [hep-ph/0703058].
- [20] N. Kauer, *Narrow-width approximation limitations*, Phys. Lett. B **649** (2007) 413 [hep-ph/0703077].
- [21] N. Kauer, *A threshold-improved narrow-width approximation for BSM physics*, JHEP **0804** (2008) 055 [arXiv:0708.1161 [hep-ph]].
- [22] C. F. Uhlemann and N. Kauer, *Narrow-width approximation accuracy*, Nucl. Phys. B **814** (2009) 195 [arXiv:0807.4112 [hep-ph]].

- [23] N. Kauer and D. Zeppenfeld, *Finite-width effects in top quark production at hadron colliders*, Phys. Rev. D **65** (2002) 014021 [hep-ph/0107181].
- [24] S. Goria, G. Passarino and D. Rosco, *The Higgs boson lineshape*, arXiv:1112.5517 [hep-ph].
- [25] G. Passarino, C. Sturm and S. Uccirati, *Higgs pseudo-observables, second Riemann sheet and all that*, Nucl. Phys. B **834** (2010) 77 [arXiv:1001.3360 [hep-ph]].
- [26] S. Actis and G. Passarino, *Two-loop renormalization in the Standard Model, Part III: Renormalization equations and their solutions*, Nucl. Phys. B **777** (2007) 100 [hep-ph/0612124].
- [27] S. Dittmaier, S. Dittmaier, C. Mariotti, G. Passarino, R. Tanaka, S. Alekhin, J. Alwall and E. A. Bagnaschi *et al.*, *Handbook of LHC Higgs cross sections: 2. Differential distributions*, arXiv:1201.3084 [hep-ph].
- [28] S. Actis, G. Passarino, C. Sturm and S. Uccirati, *NLO electroweak corrections to Higgs boson production at hadron colliders*, Phys. Lett. B **670** (2008) 12 [arXiv:0809.1301 [hep-ph]].
- [29] A. Bredenstein, A. Denner, S. Dittmaier and M. M. Weber, *Precision calculations for $H \rightarrow WW/ZZ \rightarrow 4$ fermions with PROPHECY4f*, arXiv:0708.4123 [hep-ph].
- [30] A. D. Martin, W. J. Stirling, R. S. Thorne and G. Watt, *Parton distributions for the LHC*, Eur. Phys. J. C **63** (2009) 189 [arXiv:0901.0002 [hep-ph]].
- [31] <https://twiki.cern.ch/twiki/bin/view/LHCPhysics/WW>
- [32] <https://twiki.cern.ch/twiki/bin/view/LHCPhysics/ZZ>
- [33] <http://gg2VV.hepforge.org/>
- [34] T. Binoth, M. Ciccolini, N. Kauer and M. Kramer, *Gluon-induced WW background to Higgs boson searches at the LHC*, JHEP **0503** (2005) 065 [hep-ph/0503094].
- [35] T. Binoth, N. Kauer and P. Mertsch, *Gluon-induced QCD corrections to $pp \rightarrow ZZ \rightarrow \ell\bar{\ell}\ell'\bar{\ell}'$* , arXiv:0807.0024 [hep-ph].
- [36] S. Dittmaier *et al.* [LHC Higgs Cross Section Working Group Collaboration], *Handbook of LHC Higgs Cross Sections: 1. Inclusive Observables*, arXiv:1101.0593 [hep-ph].
- [37] A. Djouadi, J. Kalinowski and M. Spira, *HDECAY: a program for Higgs boson decays in the Standard Model and its supersymmetric extension*, Comput. Phys. Commun. **108** (1998) 56 [hep-ph/9704448].
- [38] G. Aad *et al.* [ATLAS Collaboration], *Search for the Standard Model Higgs boson in the decay channel $H \rightarrow ZZ^* \rightarrow 4\ell$ with 4.8fb^{-1} of pp collision data at $\sqrt{s} = 7$ TeV with ATLAS*, Phys. Lett. B **710** (2012) 383 [arXiv:1202.1415 [hep-ex]].
- [39] S. Chatrchyan *et al.* [CMS Collaboration], *Search for the Standard Model Higgs boson in the decay channel $H \rightarrow ZZ \rightarrow 4$ leptons in pp collisions at $\sqrt{s} = 7$ TeV*, arXiv:1202.1997 [hep-ex].
- [40] G. Aad *et al.* [ATLAS Collaboration], *Search for the Standard Model Higgs boson in the $H \rightarrow WW^* \rightarrow \ell\nu\ell\nu$ decay mode with 4.7fb^{-1} of ATLAS data at $\sqrt{s} = 7$ TeV*, arXiv:1206.0756 [hep-ex].
- [41] S. Chatrchyan *et al.* [CMS Collaboration], *Search for the Standard Model Higgs boson decaying to a W pair in the fully leptonic final state in pp collisions at $\sqrt{s} = 7$ TeV*, Phys. Lett. B **710** (2012) 91 [arXiv:1202.1489 [hep-ex]].

- [42] A. J. Barr, B. Gripaios and C. G. Lester, *Measuring the Higgs boson mass in dileptonic W -boson decays at hadron colliders*, JHEP **0907** (2009) 072 [arXiv:0902.4864 [hep-ph]].
- [43] G. Aad *et al.* [ATLAS Collaboration], *Search for a Standard Model Higgs boson in the $H \rightarrow ZZ \rightarrow \ell\ell\nu\nu$ decay channel using 4.7 fb^{-1} of $\sqrt{s} = 7\text{ TeV}$ data with the ATLAS detector*, arXiv:1205.6744 [hep-ex].
- [44] S. Chatrchyan *et al.* [CMS Collaboration], *Search for the Standard Model Higgs boson in the $H \rightarrow ZZ \rightarrow 2\ell 2\nu$ channel in pp collisions at $\sqrt{s} = 7\text{ TeV}$* , JHEP **1203** (2012) 040 [arXiv:1202.3478 [hep-ex]].
- [45] D. L. Rainwater and D. Zeppenfeld, *Observing $H \rightarrow W^*W^* \rightarrow e^\pm\mu^\mp p_T$ in weak boson fusion with dual forward jet tagging at the CERN LHC*, Phys. Rev. D **60** (1999) 113004 [Erratum-ibid. D **61** (2000) 099901] [hep-ph/9906218].